Int. J. Heat Mass Transfer. Vol. 30, No. 1, pp. 93–107, 1987
Printed in Great Britain

0017–9310/87 $3.00 + 0.00
Pergamon Journals Ltd.

Thermogravitational and thermocapillary convection heat transfer in concentric and eccentric horizontal, cylindrical annuli filled with two immiscible fluids*

U. PROJAHN† and H. BEER

Institut für Technische Thermodynamik, Technische Hochschule Darmstadt, Petersenstrasse 30, 6100 Darmstadt, Federal Republic of Germany

(*Received* 19 *February* 1986)

Abstract—Laminar thermogravitational convection in concentric and eccentric horizontal, cylindrical annuli, filled with two immiscible fluids (water/air, water/silicon oil 10, water/silicon oil 100, Freon 113/water) is studied numerically. Streamline and temperature distributions, local and average equivalent thermal conductivities are obtained over a wide range of Rayleigh number. The influence of thermocapillary convection (Marangoni convection) is similarly demonstrated for the water/air system in an annular enclosure.

1. INTRODUCTION

BUOYANCY-driven convective heat transfer in a cavity filled with two immiscible fluids of different density is of great importance for many natural and industrial processes. Among other technical applications, the processing of metals, semiconductors, ceramics and polymers involves molten and vapor phases. The fluid mechanics of such technical processes, the origins and consequences of convective transport, however, are not adequately understood. Moreover gravity is not the only source of convective motions. It is of minor influence if the dimensions of the fluid system are small or if the system is exposed to micro-gravity conditions. Under these circumstances thermocapillary convection, induced by a surface tension gradient, is dominant. This kind of free convection, sometimes referred to as Marangoni convection, is nowadays of wide interest to the future possibility of material processing in space. The research activities on this subject may be seen from the large number of experiments performed during the flights of sounding-rockets (NASA SPAR and TEXUS flight experiments) [1] and in the special 'Fluid Physics Module' during D1 mission in Spacelab a few months ago.

The objective of the present study, divided into two sections, is to gain some insight into fluid motion and heat transfer phenomena if one or both types of convection, mentioned above, occur. The system under consideration consists of an annulus between two coaxially arranged, circular cylinders filled with two dissimilar fluids. Whereas the second section will be concerned with Marangoni convection and its influence on buoyancy-driven convection, the first section deals with thermogravitational convection taking into account various fluid combinations and eccentricities of the inner cylinder.

Due to the fact that the geometric shape of the system under consideration is connected with numerous technical applications, extensive experimental and theoretical work has been done during the last half of the century to investigate one-phase fluid motion and heat transfer in horizontal enclosures of concentric and eccentric cylindrical, annular shape. Comprehensive literature surveys on natural convection in such systems were given by Kuehn and Goldstein [2] for early works and by Projahn and Beer [3] for recently published results, including especially all works considering the influence of eccentricity and Prandtl number.

Investigations concerning heat and fluid flow phenomena caused by natural convection in systems containing multiple fluid layers are scarce. A review on the existing literature may be found in ref. [4]. In this work Projahn and Beer performed a theoretical and experimental study on transient and steady-state natural convection heat transfer from a vertical, flat plate partially immersed in water. Recently heat transfer results for a closed, square container filled with a liquid and a gas were published by Oosthuizen and coworkers [5,6].

Although the transport phenomena in horizontal annuli formed by two circular cylinders and filled with two immiscible fluids are very important for many technical applications, no studies of the problem addressed in this paper seem to be available in the literature.

*This contribution is dedicated to Professor F. Bošnjaković on the occasion of his 85th birthday.

†Present address: Robert Bosch GmbH, Dept. K5/EMF, P.O. Box 300220, 7000 Stuttgart 30, Federal Republic of Germany.

NOMENCLATURE

a thermal diffusivity
$\mathscr{A}^{\pm}$ abbreviation, $[J(d^{21}-g_{12}d^{22}/g_{11}]^{\pm}$
$\mathscr{B}^{\pm}$ abbreviation, $[T_{,2}-g_{12}T_{,1}/g_{11})/J]^{\pm}$
Bo Bond number, $\hat{g}(\rho^{-}-\rho^{+})L^2/\sigma$
d^{ij} deformation tensor
D diameter
g determinant of the metric tensor
$\mathbf{g}_i$ covariant basis vector
$\hat{g}$ acceleration of gravity
g_{ij}, g^{ij} co- and contravariant components of the metric tensor
G region
Gr Grashof number, Ra/Pr
h film heat transfer coefficient
J Jacobian of transformation, $\sqrt{g}$
k thermal conductivity
K_1–K_5 property ratios
L gap width, R_o-R_i
Ma Marangoni number, equation (10d)
n coordinate in normal direction
Nu Nusselt number, hL/k^{-}
p pressure
Pr Prandtl number, equation (6)
R radius
Ra Rayleigh number, equation (7)
s arc length
t time
T temperature
w^i contravariant velocity component, $(w^1, w^2) \equiv (u, v)$
x^i Cartesian coordinates, $(x^1, x^2) \equiv (x, y)$
$|_i$ covariant derivative with respect to ξ^i.

Greek symbols
β thermal expansion coefficient
ε_v vertical displacement of inner cylinder
ξ^i curvilinear coordinate system, $(\xi^1, \xi^2) \equiv (\xi, \eta)$
Λ equivalent thermal conductivity
μ dynamic viscosity
ν kinematic viscosity
ρ density
σ surface tension
φ angle (Fig. 1)
ϕ angle of gravity
ψ streamfunction.

Subscripts
$,i$ derivative with respect to ξ^i
$,t$ derivative with respect to t
A area
c cold, conduction
h hot
i inner cylinder
o outer cylinder
tot total.

Superscripts
$+$ refers to the lighter fluid
$-$ refers to the heavier fluid
$\bar{}$ mean value.

2. PROBLEM FORMULATION AND NUMERICAL SOLUTION

The problem under consideration is that of two-dimensional, laminar convection in two immiscible fluids of different density enclosed between two horizontal, concentric or eccentric cylinders. A schematic representation of the geometric arrangement is depicted in Fig. 1. In the case of eccentricity the inner cylinder is displaced up- or downwards along the vertical centerline by the distance $\varepsilon_v \lesseqgtr 0$. The heavier fluid, denoted by $(-)$, fills the lower part of the annulus, so that the interface coincides with the horizontal centerline of the inner cylinder. The surface between the two fluids is assumed to be flat and to remain unchanged under dynamical conditions. The first assumption is correct if the contact angle between solid and fluid is equal to $\pi/2$ and may be applied approximately for other angles if the Bond number Bo is large. Due to the small velocities occurring in natural convection processes, the second assumption implies no restriction of the model. Moreover it is assumed that both cylinders are maintained at different uniform temperatures $T_i > T_o$. At the solid boundaries the hydrodynamic no-slip condition ($w^i = 0$) is applied. Furthermore, the flow is symmetrical about a vertical plane through the axis of the cylinder. Accordingly, attention is confined to the range $0 \leqslant \varphi \leqslant \pi$. All fluid properties are taken to be constant except the density of the fluids, for which the validity of the Oberbeck–Boussinesq approximation is adopted. Further assumptions are neglecting viscous dissipation and compressibility effects.

Because generality was the objective of the code developed, the grid generation technique proposed by Thompson *et al.* [7] was applied to eliminate the difficulties associated with the geometric shape of the solution domain. Compared with other transformation techniques, which are often valid only for a single class of geometries, the proposed method has the great advantage that many geometric configurations of different kind can be treated with just the one computer program.

Employing general coordinate systems, the conservation equations for mass, momentum and energy, governing the problem under study, have to be for-

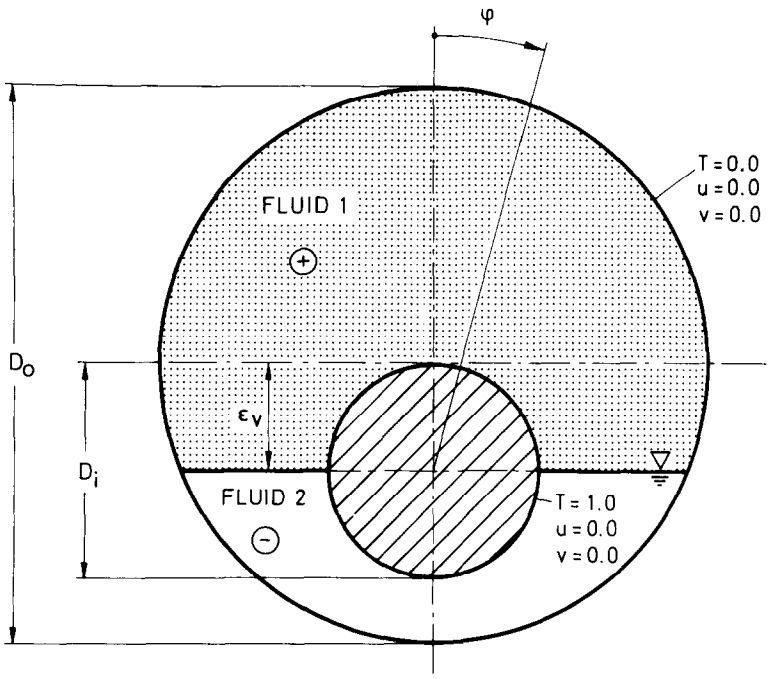

FIG. 1. Schematic representation of the problem under consideration with boundary conditions.

mulated for a general Euclidean reference frame. Suitably, general tensor notation—as used, for example, in ref. [8]—is applied. Introducing the following abbreviations

$$K_1 = \rho^-/\rho^+;\ K_2 = \nu^+/\nu^-;\ K_3 = \beta^+/\beta^-;$$
$$K_4 = a^+/a^-;\ K_5 = k^+/k^- \quad (1)$$

the governing equations for the present problem and for the fluids (+) and (−) are then given in nondimensional form as (a detailed derivation of the general conservation equations may be found in [9]):

mass: $$(Jw^i)_{,i} = 0 \quad (i = 1,2) \quad (2)$$

momentum:

$$\left[w^i_{,t} + \frac{1}{J}(Jw^iw^j)|_j + \begin{Bmatrix} K_1 \\ 1 \end{Bmatrix} g^{ij}p_{,j} + \begin{Bmatrix} K_2 \\ 1 \end{Bmatrix} \frac{Pr^-}{J}(Jd^{ij})|_j + \begin{Bmatrix} K_3 \\ 1 \end{Bmatrix} Ra^-\,Pr^-\,T\Phi^i\right]\mathbf{g}_i = 0 \quad (i,j = 1,2) \quad (3)$$

where $$d^{ij} = w^j|_k g^{ki} + w^i|_k g^{kj}$$

and $$\Phi^i = \xi^i_{,x}\cos\phi + \xi^i_{,y}\sin\phi$$

energy:

$$T_{,t} + \frac{1}{J}(Jw^iT)_{,i} - \begin{Bmatrix} K_4/J \\ 1/J \end{Bmatrix}(Jg^{ij}T_{,j})_{,i} = 0 \quad (i,j = 1,2). \quad (4)$$

In order to obtain equations (2) and (3) dimensionless variables are used. The scaling factors are $L = R_o - R_i$ for space coordinates, L^2/a^- for time, ν^-/L for velocity and $L^2/(\rho a^2)^-$ for pressure. It should be noted that the thermophysical properties of the heavier fluid (−) are chosen for reference to obtain consistent dimensionless equations for both fluid regions. Furthermore, a nondimensional temperature is defined by

$$T \leftarrow \frac{T - T_c}{T_h - T_c} \quad (5)$$

where $T_h = T_i$ and $T_c = T_o$ are the temperatures of the inner and outer cylinder, respectively. With these nondimensional variables two dimensionless numbers are introduced:

Prandtl number $$Pr^- = \nu^-/a^- \quad (6)$$

Rayleigh number

$$Ra^- = Gr^-Pr^- = \hat{g}\beta^-(T_h - T_c)L^3/\nu^-a^-. \quad (7)$$

In order to solve equations (2)–(4) appropriate boundary conditions have to be specified.

(a) *Cylinder walls* ($0 < \varphi < \pi$). They are rigid (no slip boundary condition) and at a prescribed temperature, i.e.

$$R = R_i:\ w^i = 0 \quad (i = 1,2);\ T = 1 \quad (8a)$$

$$R = R_o:\ w^i = 0 \quad (i = 1,2);\ T = 0. \quad (8b)$$

(b) *Symmetry lines* ($\varphi = 0,\ \pi$). For a line of symmetry $\xi^1 = \text{const.}$ the following conditions, which can be deduced directly from symmetry arguments, result:

no normal velocity component:

$$w^1/\sqrt{g^{11}} = 0 \tag{9a}$$

continuity of tangential velocity component:

$$\frac{g^{1j}}{\sqrt{g^{11}}}\left(\frac{g_{2i}}{\sqrt{g_{22}}}w^i\right)_{,j} = 0 \quad (i,j = 1,2) \tag{9b}$$

continuity of heat flux:

$$\frac{g^{1i}}{\sqrt{g^{11}}}T_{,i} = 0 \quad (i = 1,2). \tag{9c}$$

(c) *Interface* ($\varphi = \pi/2$). General boundary conditions for the fluid–fluid interface could be obtained by making available complete balance equations for the interface phase, which is considered as a thin shell in the three-dimensional Euclidean space [9]. Using this equation one would have to face the question of interface properties, e.g. 'interface viscosity', 'interface thermal conductivity', etc., which are not known, even their order of magnitude. For simplification the interface is assumed to be singular, resulting in the following dimensionless set of coupling conditions for the two phases (+) and (−):

Interface: coordinate line $\xi^2 = \text{const.}$

$$(w^1)^+ = (w^1)^- \quad \text{(no slip)} \tag{10a}$$

$$(w^2)^+ = (w^2)^- = 0 \quad \text{(no penetration)} \tag{10b}$$

$$(K_2/K_1)\mathscr{A}^+ - \mathscr{A}^- + Ma^- T_{,1}/\sqrt{g_{11}} = 0 \quad \text{(momentum conservation)} \tag{10c}$$

where

$$Ma^- = (\mathrm{d}\sigma/\mathrm{d}T)\Delta T L/a^-\mu^- \quad \text{(Marangoni number)} \tag{10d}$$

$$T^+ = T^- \quad \text{(continuity of temperature)} \tag{10e}$$

$$K_5\mathscr{B}^+ - \mathscr{B}^- = 0 \quad \text{(continuity of heat flux)}. \tag{10f}$$

It should be noted, however, that the balance equations of momentum yield two boundary conditions, where the equation describing the contour of the interface is omitted due to the assumption of an undeformable interface. The governing set of equations (2)–(4) in the primitive variable formulation, together with a Poisson equation for pressure, which replaces the continuity equation (2), are solved numerically by applying the finite-difference method. To avoid oscillating variable fields, the variables are located on staggered grids (MAC-scheme). Because only steady-state conditions are of interest for the present study, the false transient technique is employed to accelerate convergence. Further details concerning discretization, arrangement of the variables and numerical methods used to solve the resulting sets of algebraic equations may be found in ref. [9].

Employing finite-difference techniques, the solution domain G has to be covered by a system of coordinate lines. As pointed out, general domains of complex shape could easily be handled by applying bodyfitted coordinate systems. Typical grids, numerically generated as solution of an elliptic boundary-value problem, are shown in Fig. 2. In order to get high resolution in regions where steep gradients of the variables can be expected, the coordinate lines are clustered there. As a compromise between accuracy and computational costs, grids with the following number of nodal points are used:

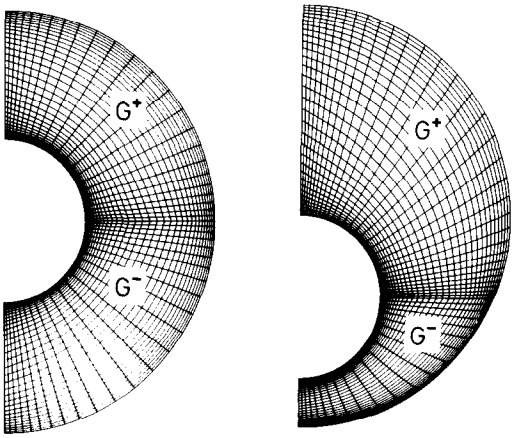

FIG. 2. Grid system.

$\varepsilon_v/L = 0.625$ $\quad G^-/G^+$: $(33\times33, 33\times21)$

$\varepsilon_v/L = 0.0$ $\quad G^-/G^+$: $(33\times25, 33\times25)$

$\varepsilon_v/L = -0.625$ $\quad G^-/G^+$: $(33\times21, 33\times33)$.

3. EQUIVALENT THERMAL CONDUCTIVITY

Studying heat transfer in cylindrical annuli, heat transfer rates are usually expressed in terms of the equivalent thermal conductivity. This dimensionless quantity is equal to the ratio of total heat transfer to heat transfer due to heat conduction only, i.e.

$$\Lambda^\pm = Nu^\pm/Nu_c \tag{11}$$

where the Nusselt number Nu may be calculated from the temperature gradient normal to the cylinder wall ($\xi^i = \text{const.}$)

$$Nu^\pm = h^\pm L/k^- = \begin{Bmatrix} K_5 \\ 1 \end{Bmatrix} \frac{g^{ij}}{\sqrt{g^{ii}}} T_{,j} \quad (j = 1,2). \tag{12}$$

The Nusselt number Nu_c for pure heat conduction is based on the concentric annulus case and results in

$$Nu_c = h_c L/k^- = L/[R_{(i,o)} \ln(R_o/R_i)]. \tag{13}$$

For the problem under consideration, where the annulus contains two immiscible fluids, the following definition of the equivalent conductivity is introduced. It takes into account the ratio of the wetted cylinder surfaces $A^\pm$ to the total area A_{tot}

$$\Lambda_A^\pm = \Lambda^\pm A^\pm/A_{tot}. \tag{14}$$

In order to express the overall heat transfer across a given surface, the global equivalent conductivity $\bar{\Lambda}$ has to be calculated. With the definitions given above one obtains by integration:

$$\bar{\Lambda} = \left(\int_{A^+} \Lambda^+ \, ds + \int_{A^-} \Lambda^- \, ds \right) \Big/ A_{tot}$$

$$= \bar{\Lambda}_A^+ + \bar{\Lambda}_A^- = \overline{Nu}/Nu_c \quad (15)$$

where s denotes the arc length along the cylinder surface.

4. RESULTS AND DISCUSSION

Numerical solutions to the problem of heat transfer due to buoyancy-driven and thermocapillary convection have been obtained for a diameter ratio $D_o/D_i = 2.6$. The majority of the computations have been performed for a concentric arrangement of both cylinders, whereas only for the case of pure thermogravitational convection has eccentricity been introduced as a further parameter.

All results are first presented qualitatively in the form of streamline and isotherm patterns and then quantitatively by the distribution of the local equivalent conductivity Λ_A which is supplemented by the global values $\bar{\Lambda}$. Because all variables are nondimensionalized with the properties of the heavier fluid, the problem-dependent Rayleigh number used for the calculations is Ra^-, characterizing fluid flow and heat transfer in the region G^-. The parameter Ra^+ may be calculated from

$$Ra^+/Ra^- = K_3/K_2K_4. \quad (16)$$

For the fluid combination air and water the following relation holds

$$Ra^+ = 7.23 \times 10^{-3} Ra^- \quad (17)$$

i.e. both fluid segments are dominated by quite different flow regimes for the majority of Rayleigh numbers Ra^- studied.

4.1. *Thermogravitational convection*

The investigations concerning thermogravitational convection only ($Ma^- = 0$) have been performed for eccentricities

$$\varepsilon_v/L = 0.625; \quad 0.0; \quad -0.625$$

for Rayleigh numbers in the range $10^3 \leqslant Ra^- \leqslant 10^7$ and for systems containing various fluid combinations. For the numerical calculations the thermophysical properties given in Table 1 based on a reference temperature of 20°C have been used.

The motion of the fluid and the resulting temperature field provides one way to observe local effects of buoyancy. In Fig. 3, these effects are vividly portrayed in plots of lines of constant streamfunction and isotherms for a concentric arrangement ($\varepsilon_v/L = 0.0$) of both cylinders and the fluid combination water/air. As mentioned earlier, the problem under consideration is symmetrical with respect to a vertical axis, and it was found advantageous to reproduce the computer results on a single graph with the flow pattern on the right half of the cavity and isotherms on the left half. It is obvious that heat transfer in both fluid parts depends mainly on heat conduction for $Ra^- = 10^3$ ($Ra^+ \simeq 7$). Due to a stronger fluid motion in the water-filled portion of the annulus and because both convective cells have the same sense of rotation, a secondary flow cell is induced near the interface of the air-filled space. At the interface fluid motion is directed towards the cold wall, leading to a concentration of the isotherms at this point. With increasing Rayleigh number this effect is enhanced and the secondary cell is pushed aside due to an intensified convective motion in the upper part of the annulus. The transition from conduction to the laminar boundary-layer regime is terminated in the water segment at $Ra^- = 10^5$. In the part containing air, heat transport is dominated by conduction up to $Ra^- = 10^5$ ($Ra^+ = 723$). Only when the Rayleigh number is increased further does the transport mechanism change. For $Ra^- = 10^7$ ($Ra^+ = 73{,}200$) the distribution of the fields of variables indicates that the heat transfer characteristics in both fluids may be related to the boundary-layer regime.

The influence on heat transfer is evidenced in more detail by the distribution of the local equivalent conductivity along the outer and inner cylinder, depicted in Fig. 4. In each case the left half represents the conductivity within the fluid (+) and the right half that within the fluid (−). It has to be emphasized that different scales are valid in both halves. For $Ra^- = 10^3$ heat transfer is dominated by heat conduction. It is worth mentioning that in the case of pure heat conduction the local equivalent conductivities Λ_A per definition [equation (14)] are equal to 0.5 and $0.5K_5$, respectively. With increasing Rayleigh numbers convective motion is enhanced, leading to a dis-

Table 1

Fluid(−)/fluid(+)	K_1	K_2	K_3	K_4	K_5	Pr^+/Pr^-
water/air	849.6	16.82	18.5	152.2	0.043	0.1
water/silicon oil 10	1.06	11.20	4.18	0.65	0.213	15
water/silicon oil 100	1.03	111.99	3.75	0.71	0.246	136
Freon 113/water	1.58	2.22	0.133	2.19	6.45	$\simeq 1$

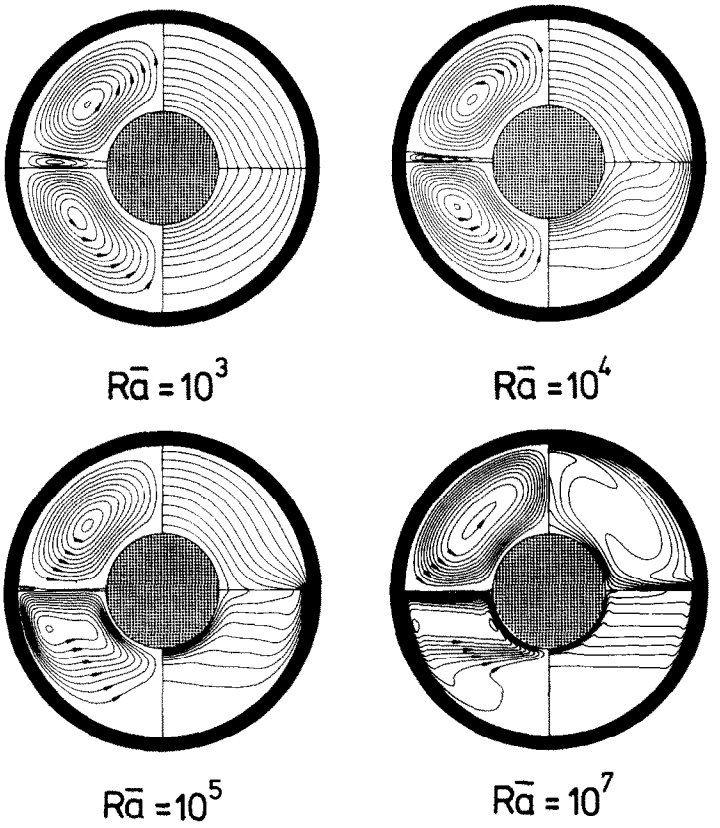

FIG. 3. Lines of constant streamfunction (left) and temperature (right) for various Rayleigh numbers and the system water/air ($Pr^+ = 0.7$; $Pr^- = 7.0$; $\varepsilon_v/L = 0$).

tinct local distribution of Λ_A, with increasing maxima at the interface. As a result of thermal stratification, heat transfer is decreased strongly in the lower part of the fluid (−), whereas another maximum occurs at the outer cylinder in the upper part of the annulus (air) due to the stagnation flow. Heat transfer at the inner cylinder is hampered for small Rayleigh numbers ($Ra^- = 10^3$; 10^4) as the air warms up flowing along the interface. Only after an intensification of the convective flow is heat transfer increased at the inner cylinder, leading to nearly identical values at the interface and at the upper stagnation point. In the upper part (air) the maximum values appear in the reversal zone of the circulating air flow ($\varphi = 60°$). In the water-filled space, maximum values are registered at the lower stagnation point of the inner cylinder.

Figure 5 depicts the flow and isotherm patterns obtained for the two eccentric configurations under study and three selected Rayleigh numbers. For $\varepsilon_v/L = -0.625$ the convective motion in the air-filled space is stronger than for a concentric arrangement of the cylinders, resulting in a smaller secondary flow cell above the interface. The presence of a stronger fluid motion may also be seen from the distribution of the isotherms. The deviations from the conduction solution for small and intermediate Rayleigh numbers as well as the thermal plume for high Rayleigh numbers are more pronounced than in Fig. 3. For the flow regimes in the water layer no significant differences to those of the concentric case are detectable. The effect of positive eccentricity is discernible from the dimensions of the secondary cells induced by the water motion across the interface. It is evident that this geometric configuration of two cylinders inhibits convective motion in the upper part of the annulus. This is easily recognized by the temperature fields for $Ra^- = 10^3$ and 10^5 which remain nearly unchanged, showing that heat conduction is the dominating heat transfer mechanism. Increasing the Rayleigh number up to 10^7, convection becomes stronger and heat transfer is characterized by thin boundary layers along the cylinder walls. The boundary layer around that part of the inner cylinder which is exposed to air separates at $\varphi \simeq 30°$ and forms two counter-rotating cells. Quite similar multicellular flows were found to exist for the same geometric configuration when the annulus is filled with a homogeneous fluid, for Prandtl numbers in the range $0.7 \leqslant Pr \leqslant 100$ [3,10].

In comparison with the concentric case the large stagnant fluid region below the inner cylinder is remarkable.

Local equivalent conductivities for eccentric con-

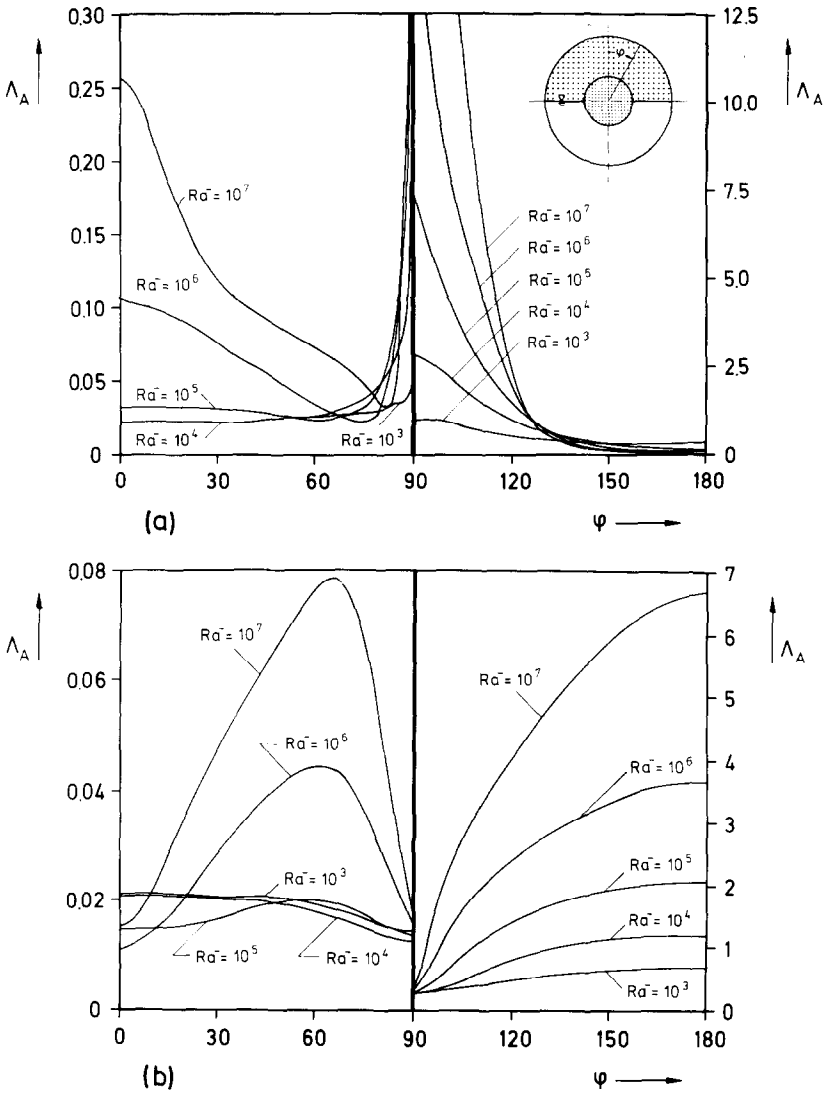

FIG. 4. Local distribution of the equivalent thermal conductivities along the outer (a) and inner (b) cylinder for various Rayleigh numbers and the system water/air.

figurations are plotted in Fig. 6. Whereas heat transfer rates in the air-filled part of the annulus for negative eccentricity do not deviate strongly from those for the concentric configuration, the maximum heat transfer rates shift to a position below the interface in the water layer. Differences to the concentric arrangement may also be encountered for the lighter fluid at the outer cylinder for positive eccentricity (Fig. 6c). In this case the second relative maximum forms at $\varphi = 30°$ for $Ra^- \geqslant 10^6$, as a consequence of the secondary roll cell. This behavior causes the formation of two maxima (Fig. 6d) at the inner cylinder for $Ra^- \geqslant 10^6$; these are located at the upper stagnation point and at the point of impact of the circulation flow near the interface.

In Fig. 7 the mean equivalent conductivity $\bar{\Lambda}$, averaged with respect to both fluids, is plotted vs Ra^-, defined with the properties of fluid(−) (water). The symbols represent the theoretical/numerical data which can be approximated quite well by a straight line for $Ra^- \geqslant 10^4$ which yields the correlation

$$\bar{\Lambda} = 0.098(Ra^-)^{0.242} \quad (10^4 \leqslant Ra^- \leqslant 10^7). \quad (18)$$

The maximum deviation amounts to +7.8% for $Ra^- = 10^4$ and $\varepsilon_v/L = -0.625$. If equation (18) is restricted to $Ra^- \geqslant 10^5$, the maximum deviation is decreased to +3.2% ($Ra^- = 10^7$, $\varepsilon_v/L = +0.625$). For comparison, mean equivalent conductivities for a homogeneous fluid in a horizontal, concentric annulus—as determined in refs. [3,10]—are plotted in Fig. 7. This demonstrates that a partially filled annulus (water/air) causes a drastic deterioration in heat transfer. In contrast to the heat transfer in homogeneous fluids, where only in the case of a vertical downward

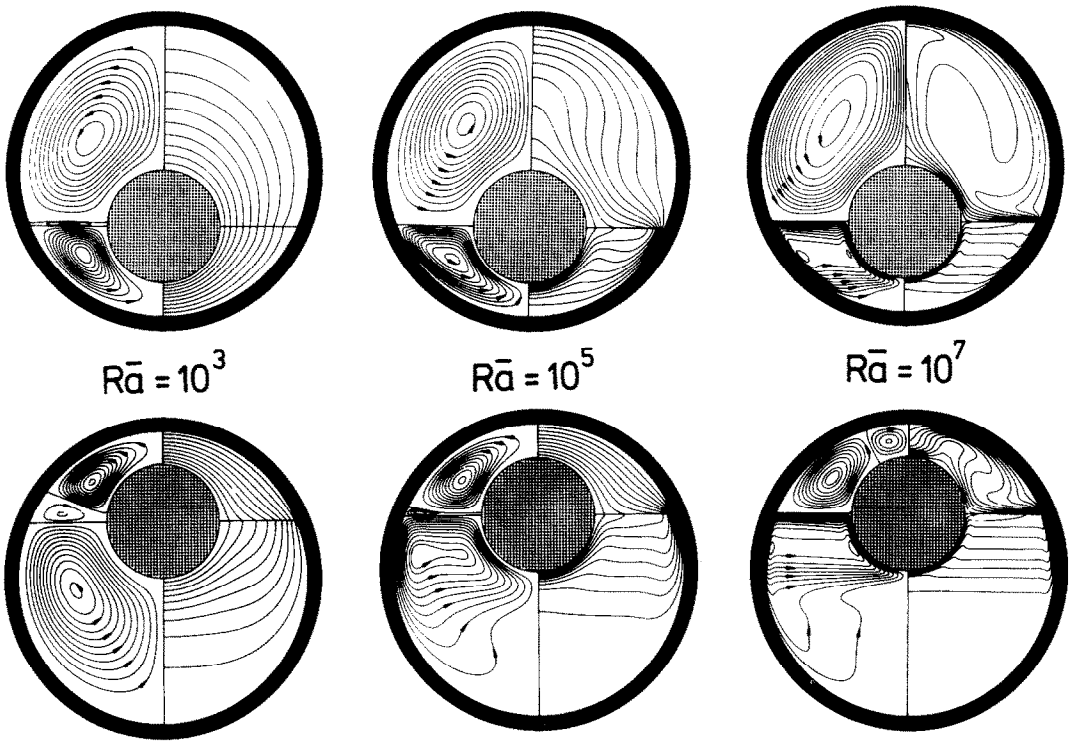

FIG. 5. Streamlines (left) and isotherms (right) for various Rayleigh numbers and eccentricities for the system water/air ($Pr^+ = 0.7$; $Pr^- = 7.0$). Top row: $\varepsilon_v/L = -0.625$; bottom row: $\varepsilon_v/L = +0.625$.

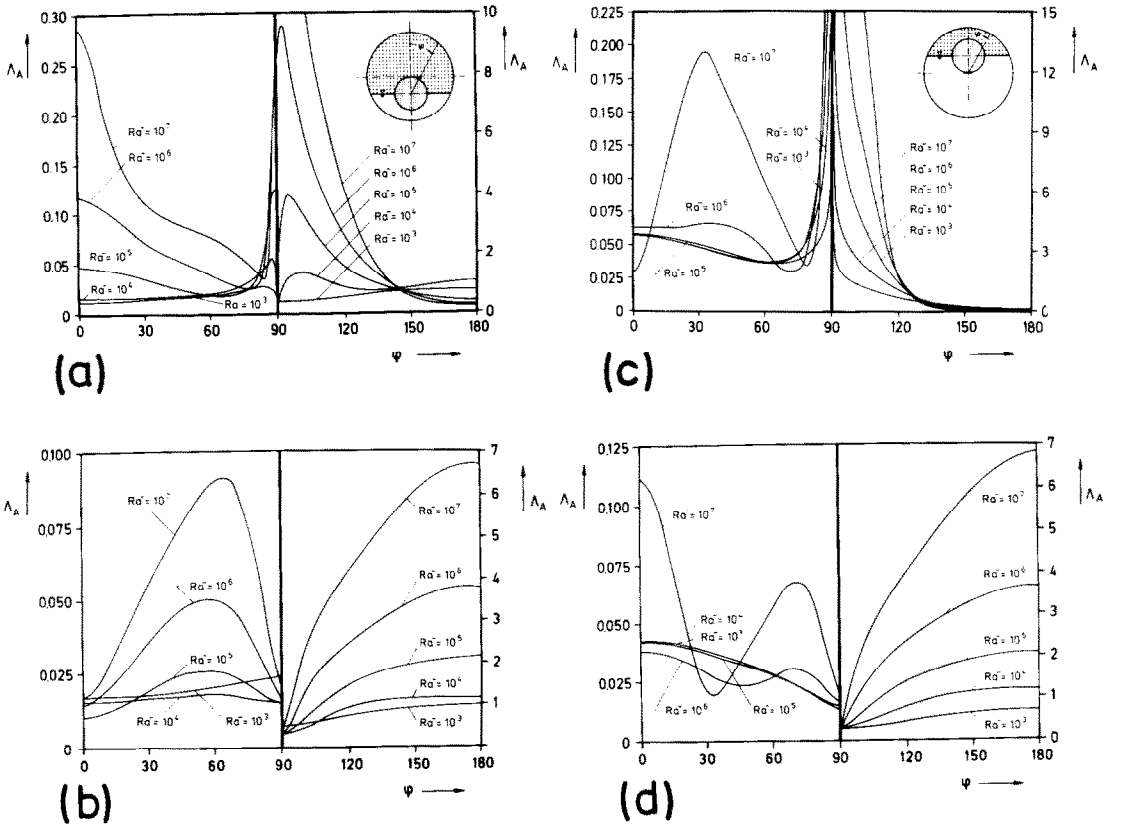

FIG. 6. Local equivalent thermal conductivities along the outer (a,c) and inner (b,d) cylinder for various Rayleigh numbers and the system water/air. Left: $\varepsilon_v/L = -0.625$; right: $\varepsilon_v/L = +0.625$.

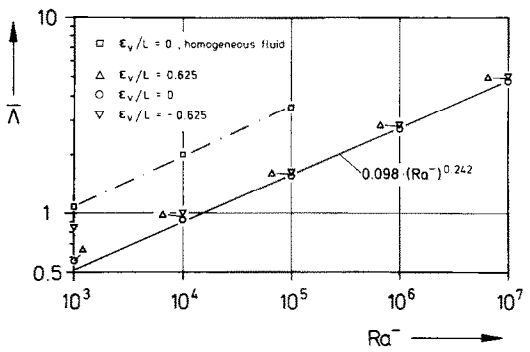

FIG. 7. Mean equivalent thermal conductivities as a function of the Rayleigh number for the concentric and eccentric annulus and the system water/air ($\varepsilon_v/L = +0.625$, 0, -0.625).

displacement of the inner cylinder could an enhancement of heat transfer be registered, there results a slight increase of $\bar{\Lambda}$ (1–5%) in a partially filled annulus (water/air) for all cases of eccentricity as compared with the concentric configuration.

The influence of different thermophysical properties on the transport phenomena was investigated for a concentric arrangement of the cylinders and for the fluid combinations tabulated above. For reason of brevity the results are restricted to solutions for $Ra^- = 10^5$ ($Ra_1^+ = 723$; $Ra_2^+ = 57{,}200$; $Ra_3^+ = 4680$; $Ra_4^+ = 2740$). The nature of the flow pattern in the form of streamfunction and temperature distributions is shown in Fig. 8. With the exception of the secondary eddies appearing in the region G^- of the water/silicon oil systems, all lines of constant streamfunction have nearly the same structure and magnitude. The effect of stratifying the heavier fluid by a more viscous fluid is elucidated by the behavior of the isotherms. While the lines of constant temperature attain their maximum depth of penetration exactly at the interface for the combination water/air, this point is located some distance beneath the interface if the upper fluid has a higher viscosity. As a consequence the isotherms are bent backwards in the vicinity of the interface. This result is always obtained if the separating plane between air and water is considered to be a solid interface [4]. For the water/air system the absolute maximum heat transfer along the lower part of the outer cylinder was found at the interface. In contrast to that the maximum for the other fluid combinations may be expected at $\varphi \simeq 100°$.

Due to the different Rayleigh numbers Ra^+, quite different regimes occur in the annulus above the interface. While heat transfer is dominated by heat conduction in the space containing air, convection affects heat transport in the remaining systems. The strongest fluid motion may be observed in that part of the annulus filled with silicon oil 10. This is recognized on the corresponding plot as a temperature inversion and

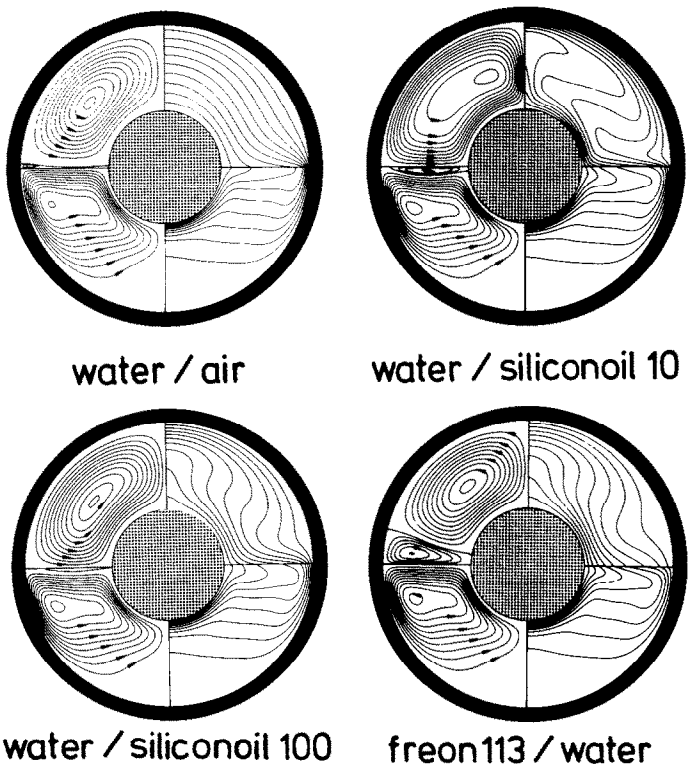

FIG. 8. Streamlines (left) and isotherms (right) for various fluid combinations and $Ra^- = 10^5$.

by the location of the convective cell center, which has moved towards $\varphi = 0°$. The motion of the fluid is strong enough to induce a secondary flow cell in the lower half of the annulus.

The influence of strongly different viscosities on the transport mechanisms may be detected by comparing the systems water/silicon oil 100 ($\mu^+/\mu^- = 109$) and Freon 113/water ($\mu^+/\mu^- = 1.4$). Although both Rayleigh numbers Ra^+, characterizing heat transfer and fluid flow in the upper half of the annulus, are of the same order of magnitude, quite different flow patterns are obtained. Due to the high viscosity of the oil the secondary flow cell forms in the fluid(−), whereas the nearly identical viscosity of Freon 113 leads to a roll cell in the upper liquid, induced by the relative strong convective motion in the Freon layer.

The local equivalent conductivities along the outer cylinder are depicted in Fig. 9. A corresponding Λ-distribution along the inner cylinder was omitted, as the principle characteristics remain unchanged as compared with the system water/air. Contrary to the common practice the equivalent conductivity Λ_A of Freon 113/water is not related to the fluid(−) but to the fluid(+) (water), in order to ensure a uniform presentation. As mentioned, the maximum conductivities occur below the interface ($\varphi \simeq$ 100–105°) except for the system water/air. The highest local heat transfer rate is achieved with the system water/air, as the circulating air flow is scarcely retarded (by virtue of the low viscosity) and therefore impinges on the outer cylinder with a higher velocity. The smallest heat transfer rate is obtained when the lower part of the annulus is filled with Freon 113, as its thermal conductivity ($K_5 = 6.45$) is considerably below that of water.

In the upper part of the annulus the highest heat transfer rates can be observed for the system Freon 113/water. In this case water is the lighter fluid at the top. The absolute maximum appears at the upper stagnation point, where the fluid which ascends from the inner cylinder impinges. From there, heat transfer rates decrease along the outer cylinder until the absolute minimum is obtained in the region of the dividing streamline of the counter-rotating eddies. This is followed by an increase up to the values at the interface. Similar behavior can be stated for the remaining fluid combinations.

Table 2

Fluid(−)/fluid(+)	$\bar{\Lambda}$
water/air	1.56
water/silicon oil 10	1.79
water/silicon oil 100	1.32
Freon 113/water	1.03

All calculated mean integral equivalent thermal conductivities $\bar{\Lambda}$ are given in Table 2. One has to recall that all values refer to the thermal conductivity of water. The results reveal that, for a given Rayleigh number ($Ra^- = 10^5$), the most intensive heat transfer can be achieved with the system water/silicon oil 10 because of a very intense convective flow in both layers. On the other hand the combination water/silicon oil 100 yields smaller values than water/air as the water flow velocity close to the interface is retarded, owing to the high viscosity of the silicon oil. The system Freon 113/water comes off worst. This is due to the low thermal conductivity of the refrigerant as well as to the water-side heat transfer which is hampered by the secondary flow cell. These results

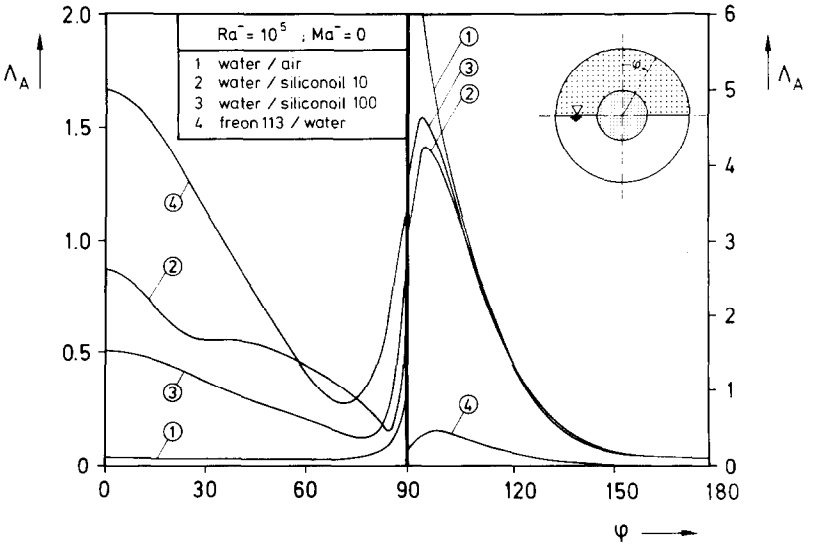

FIG. 9. Local distribution of the equivalent thermal conductivities Λ_A along the outer cylinder for various fluid combinations and $Ra^- = 10^5$.

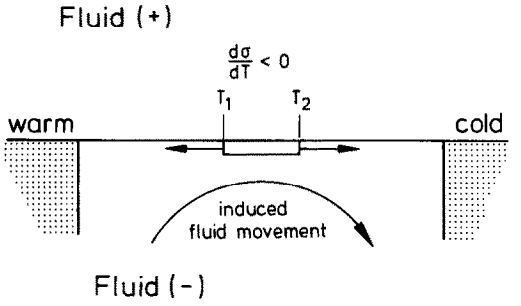

FIG. 10. Generation of an interfacial flow by a surface tension gradient.

calculated for several fluid combinations do not claim completeness, but pretend to demonstrate exemplarily the influence of different property ratios on the heat transfer mechanisms.

4.2. *Thermocapillary convection*

The transport processes so far presented are based solely on thermal conduction and natural convection due to buoyancy forces. In the case of very small dimensions or under microgravity conditions, however, a temperature gradient along the interface may induce Marangoni convection, due to the temperature dependence of the surface tension. This mechanism is explained by Fig. 10. The depicted surface element is submitted to a temperature difference $T_1 > T_2$. As the surface tension σ mostly decreases with increasing temperature, an interfacial flow will result which is directed from the warm side to the cold side of the element, i.e. from the region of low surface tension to that of high surface tension. Thus the surface tension force acting on the surface element is opposed by viscous shear stress in the adjacent bulk phases, mainly in the liquid phase. If the surface tension gradient is maintained, thermocapillary convection will develop as a continuous flow which penetrates into the fluids divided by the interface.

The subject of this chapter is the influence of an interfacial flow on heat transfer. The computation was performed for a concentric horizontal and cylindrical annulus filled half with water and half with air. As the thermophysical properties of this combination are specified in the preceding section, only the surface tension $\sigma(20°) = 7.22 \times 10^{-2}$ N m^{-1} and its dependence of temperature $d\sigma/dT = 1.75 \times 10^{-4}$ N m^{-1} K^{-1} are stated here. In order to take into account buoyancy-driven convection as well as thermocapillary convection, the two following parametric studies were performed

(1) $Ra^- = 500$;
$Ma^- = 0, -250, -500, -1000, -5000, -10{,}000$

(2) $Ma^- = -1000$; $Ra^- = 10^3, 10^4, 10^5$.

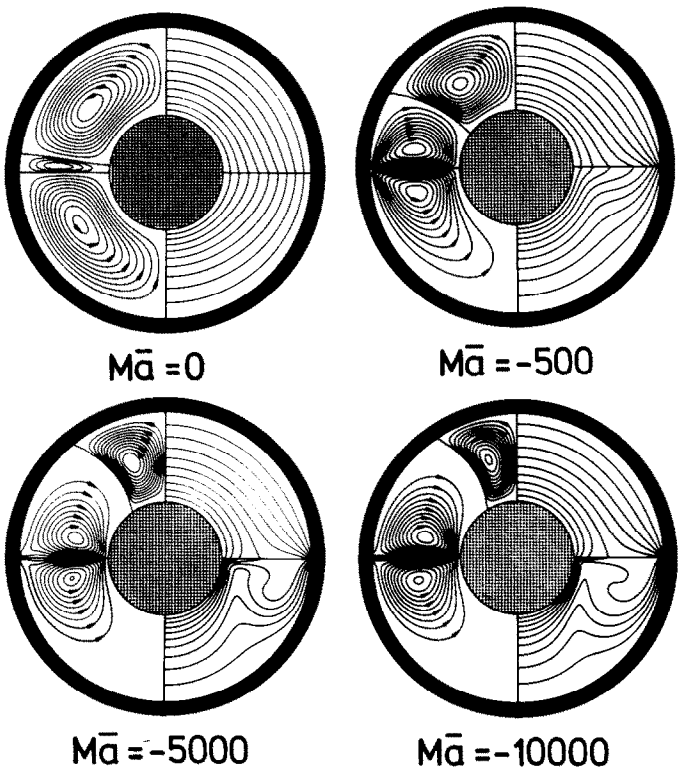

FIG. 11. Streamlines (left) and isotherms (right) for $Ra^- = 500$ ($Pr^+ = 0.7$; $Pr^- = 7.0$) and various Marangoni numbers Ma^- (system: water/air).

In both cases $Pr^+ = 0.7$ and $Pr^- = 7.0$, the Marangoni number Ma^- is defined by equation (10d).

The development of thermocapillary dominated convection ($Ma^- = -10^4$) from pure buoyancy-driven flow ($Ma^- = 0$) is vividly displayed by Fig. 11, representing the distribution of streamlines and isotherms. Considering thermogravitational convection only, the secondary eddy above the interface is weak and occupies a small area. With the onset of surface tension effects the surface velocity is enhanced and the secondary flow cell grows in strength and volume. The interface velocity increases with growing Marangoni number $|Ma^-|$. The resulting flow cells below and above the interface have nearly identical shapes and a structure which is typical for pure shear flows (e.g. driven-cavity-problem). Due to the intensified capillary flow, the flow cell induced by gravity forces is displaced more and more. For $|Ma^-| \geqslant 5000$ only a small area is occupied, indicating that thermogravitational convection is of minor importance for a ratio $|Ma^-/Ra^-| > 10$. For $Ma^- = 0$ heat transfer is dominated by heat conduction and the isotherms are nearly concentric circles. Due to the temperature gradients along the interface, statically unbalanced gradients of surface tension appear, causing a flow from the hot to the cold side. This motion leads to a contraction of the isotherms at the intersection of the interface and the outer wall. According to the strong rotary motion at higher Marangoni numbers, water is convected towards the inner cylinder, i.e. the maximum heat flux at the inner cylinder can be expected at a position close below the interface.

The phenomena described above are evidenced by the distribution of the local equivalent conductivity

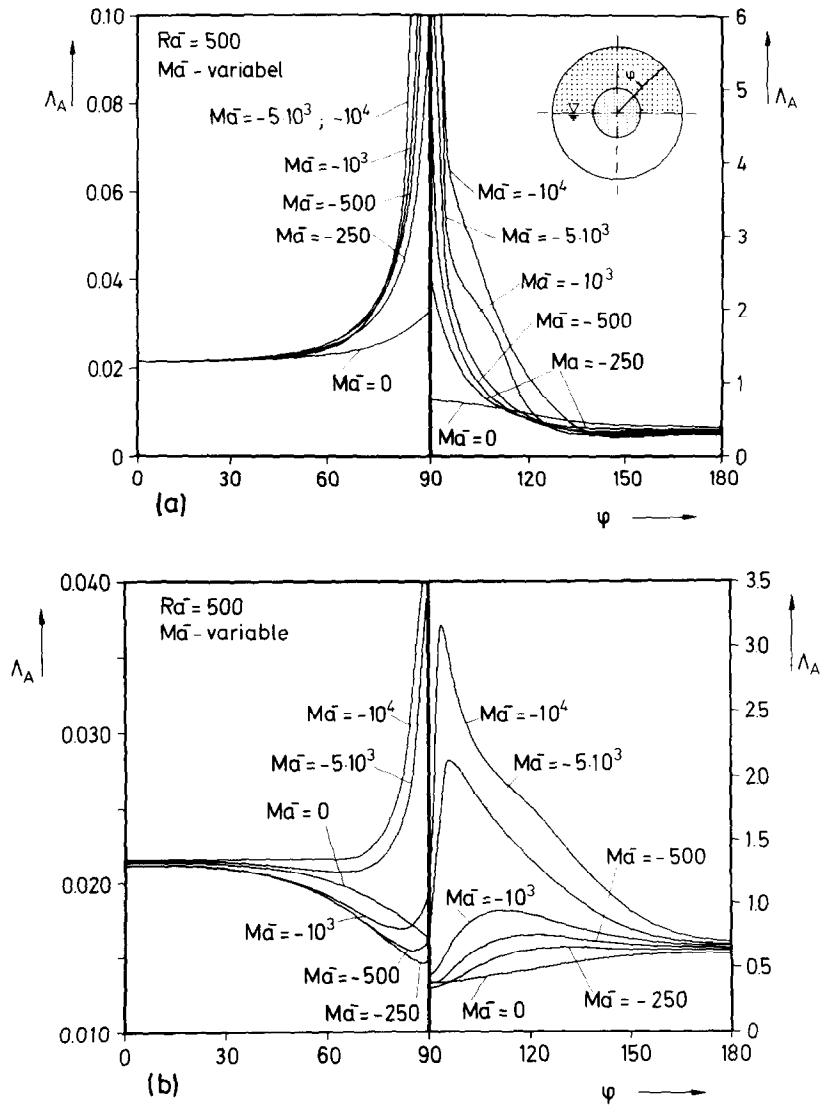

FIG. 12. Local equivalent thermal conductivities along the outer (a) and inner (b) cylinder for $Ra^- = 500$ ($Pr^+ = 0.7$; $Pr^- = 7.0$) and various Marangoni numbers Ma^- (system: water/air).

Table 3

Ma^-	0	−250	−500	−1000	−5000	−10,000
$\bar{\Lambda}$	0.539	0.615	0.682	0.791	1.156	1.454

depicted in Fig. 12. The plots reveal that Marangoni convection improves heat transfer at the outer cylinder in any case, leading to absolute maxima at the point of contact between the interface and the outer wall. This statement, however, must be qualified for the inner cylinder. For $|Ma^-| \leqslant 10^3$ the heat transfer at the air-side part of the inner cylinder is decreased. Only for $|Ma^-| \geqslant 10^3$ does the heat flux receive an enhancement.

At the circumference of the inner cylinder, wetted by water, an increasing Marangoni convection manifests itself in the formation of an absolute maximum which occurs at $\varphi \simeq 130°$ for $Ma^- = -250$ and which moves towards the interface with increasing Marangoni number. Both plots demonstrate that heat transfer at the upper and lower stagnation points is not influenced by the thermocapillary flow, which acts only about the interface.

An enhancement of the local equivalent thermal conductivity leads to an increase of the total heat flux. For $Ra^- = 500$ the mean equivalent conductivities $\bar{\Lambda}$ given in Table 3 result. Accordingly Marangoni convection causes an intensification of heat transfer by nearly 270% for the highest Marangoni number under consideration, as compared with sole thermal convection ($Ma^- = 0$). The value of $\bar{\Lambda}$ almost attains that which is achieved without Marangoni convection for $Ra^- = 10^5$ with the same geometric configuration.

In order to understand the influence of Marangoni convection on buoyancy-driven flow, a study was performed with constant Marangoni number ($Ma^- = -10^3$) and varying Rayleigh numbers ($10^3 \leqslant Ra^- \leqslant 10^5$). The results are compared with the solutions given in Section 4.1 ($Ma^- = 0$). The resulting distributions of streamfunction and isotherms are shown in Fig. 13. It is evident that the influence of thermocapillary convection decreases with increasing Rayleigh number. Consequently, for $Ra^- = 10^5$ only insignificant differences are detectable. The roll cell situated above the interface demonstrates that it

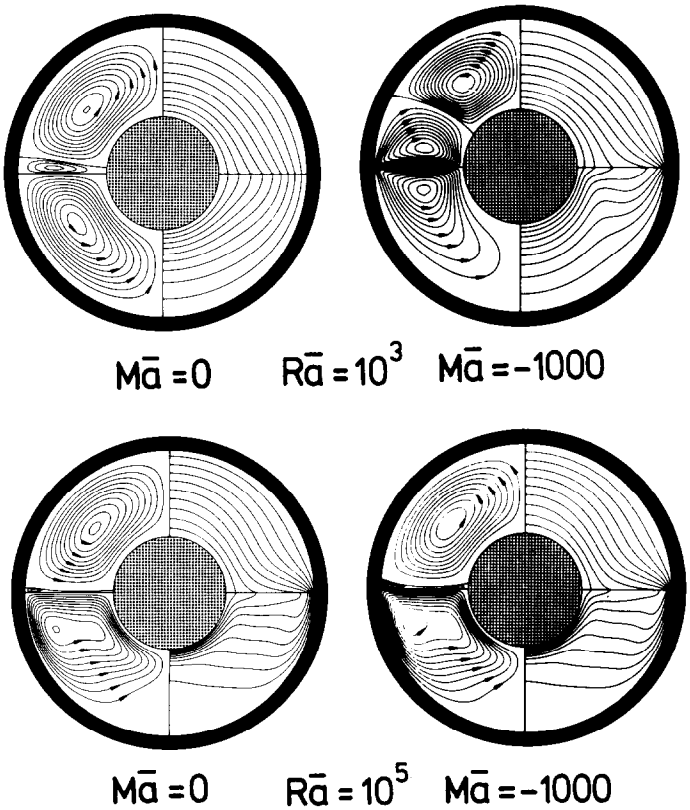

FIG. 13. Streamlines (left) and isotherms (right) for $Ma^- = 0$ (left) and $Ma^- = -1000$ (right) at various Rayleigh numbers Ra^- ($Pr^+ = 0.7$; $Pr^- = 7.0$; system: water/air).

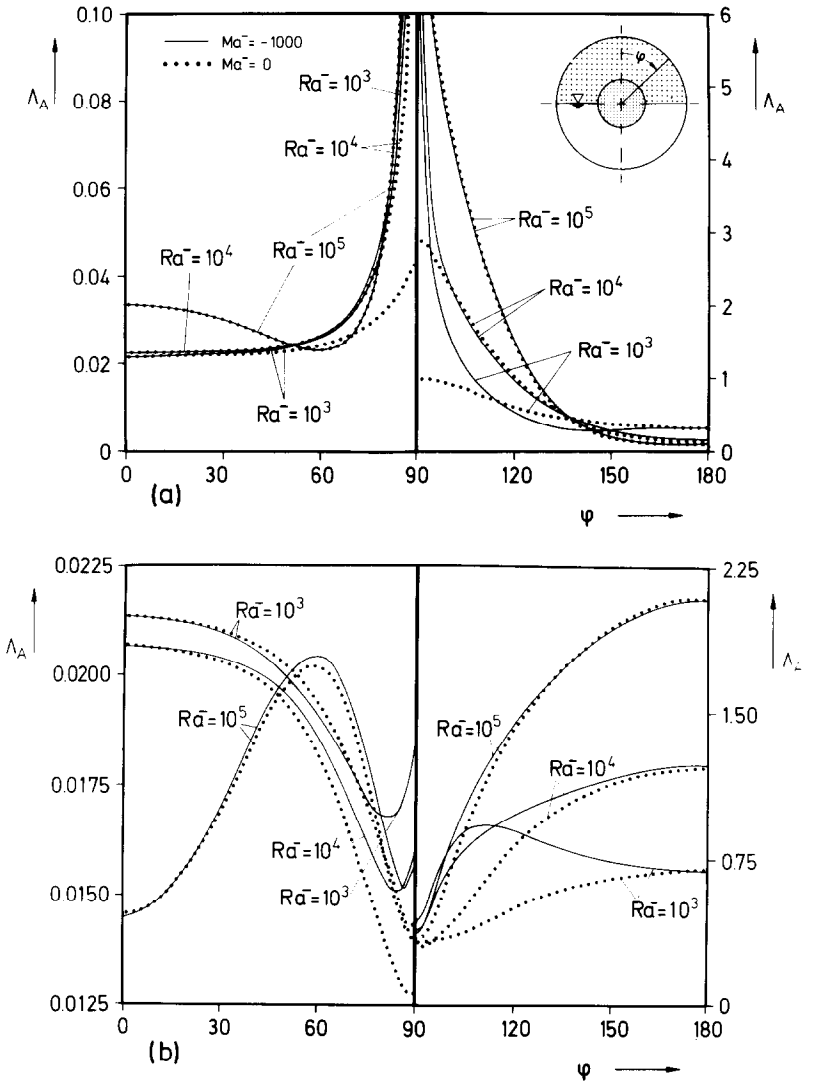

FIG. 14. Local equivalent thermal conductivity Λ_A along the outer (a) and inner (b) cylinder for $Ma^- = 0$, -1000 and various Rayleigh numbers ($Pr^+ = 0.7$; $Pr^- = 7.0$; system: water/air).

grows in strength if an interfacial velocity, arising from surface tension effects, is imposed. Due to the more powerful convective motion in the annulus caused by Marangoni convection, heat transfer is also improved, especially for low Rayleigh numbers.

This impression is confirmed by Fig. 14, where the local equivalent thermal conductivities are plotted along the inner and outer cylinder. Whereas at the upper part of the outer cylinder a considerable improvement of heat transfer can be observed only for $Ra^- = 10^3$, the corresponding values of Λ_A in the water-filled space show a clear tendency to higher maxima for $Ra^- = 10^3$ as well as for $Ra^- = 10^4$. In contrast, only a slight influence of Marangoni convection can be observed for $Ra^- = 10^5$. The plots for the inner cylinder, however, reveal a distinct influence of thermocapillary convection for all cases under consideration. Even for $Ra^- = 10^5$ an improvement can be stated near the interface. The occurrence of intense Marangoni convection at the inner cylinder is due to the strengthening of the secondary flow cell in the fluid(+) which intensifies the flow close to the inner cylinder. On the other hand the flow directed to the outer cylinder is stronger anyway, so that a velocity increase at the interface scarcely influences the temperature gradient.

Table 4

Ra^-	5×10^2	10^3	10^4	10^5
$\bar{\Lambda}$ ($Ma^- = 0$)	0.539	0.573	0.924	1.557
$\bar{\Lambda}$ ($Ma^- = -1000$)	0.791	0.796	1.046	1.609
Improvement	46.6%	38.9%	13.2%	3.3%

As a result of the present investigation the following conclusion can be made: in the case of steady flow, Marangoni convection improves heat transfer. The improvement, however, diminishes with increasing Rayleigh number. This context is displayed by the mean integral equivalent thermal conductivities listed in Table 4.

Acknowledgement—The authors wish to express their appreciation for the support of this work by the Deutsche Forschungsgemeinschaft—DFG.

REFERENCES

1. H. U. Walter, Results of material science experiments with sounding rockets, *ESA J.* **7**, 235–246 (1983).
2. T. H. Kuehn and R. J. Goldstein, An experimental and theoretical study of natural convection in the annulus between horizontal concentric cylinders, *J. Fluid Mech.* **74**, 695–719 (1976).
3. U. Projahn and H. Beer, Prandtl number effects on natural convection heat transfer in concentric and eccentric horizontal cylindrical annuli, *Wärme- u. Stoffübertr.* **19**, 249–254 (1985).
4. U. Projahn and H. Beer, Theoretical and experimental study of transient and steady-state natural convection heat transfer from a vertical flat plate partially immersed in water, *Int. J. Heat Mass Transfer* **28**, 1487–1498 (1985).
5. P. H. Oosthuizen and J. T. Paul, Heat transfer through a closed square container filled with a liquid and a gas, ASME Paper 83-WA/HT-101, ASME Winter Annual Meeting (1983).
6. P. H. Oosthuizen and D. Kuhn, Unsteady free convection heat transfer through a closed square container filled with a liquid and a gas, ASME Paper 84-HT-66, ASME 22nd National Heat Transfer Conference, Niagara Falls (1984).
7. J. F. Thompson, F. C. Thames and C. W. Mastin, Automatic numerical generation of body-fitted curvilinear coordinate systems for field containing any number of arbitrary two-dimensional bodies, *J. Comput. Phys.* **15**, 299–319 (1974).
8. W. Flügge, *Tensor Analysis and Continuum Mechanics*. Springer-Verlag, Berlin (1972).
9. U. Projahn, Numerische und experimentelle Untersuchung von stationären und instationären konvektiven Wärmetransportvorgängen in ein- und zweiphasigen Fluidsystemen. Doctoral thesis, Technische Hochschule Darmstadt (1984).
10. U. Projahn, H. Rieger and H. Beer, Numerical analysis of laminar natural convection between concentric and eccentric cylinders, *Numer. Heat Transfer* **4**, 131–146 (1981).

TRANSFERT DE CHALEUR PAR CONVECTION THERMOGRAVITATIONNELLE ET THERMOCAPILLAIRE DANS UN ANNEAU HORIZONTAL FORME DE DEUX CYLINDRES CONCENTRIQUES ET EXCENTRIQUES ET REMPLI DE DEUX FLUIDES NON MISCIBLES

Résumé—La convection laminaire naturelle (gravitationnelle) dans un anneau horizontal formé de deux cylindres concentriques et excentriques et rempli de deux fluides non miscibles (eau/air, eau/huile aux silicones 10, eau/huile aux silicones 100, Freon 113/eau) est étudiée à l'aide d'un procédé numérique. Les répartitions de la fonction de courant et des températures, les conductivités thermiques équivalentes locales et moyennes sont obtenues dans un large domaine du nombre de Rayleigh. L'influence de la convection thermocapillaire (convection de Marangoni) est démontrée sur le système eau/air pour les mêmes configurations géométriques.

WÄRMEÜBERTRAGUNG DURCH SCHWEREKONVEKTION UND THERMOKAPILLARE KONVEKTION IN EINEM MIT ZWEI NICHTMISCHBAREN FLUIDEN GEFÜLLTEN HORIZONTALEN RINGSPALT ZWISCHEN KONZENTRISCHEN UND EXZENTRISCHEN ZYLINDERN

Zusammenfassung—Mit Hilfe eines numerischen Verfahrens wird die laminare Schwerekonvektion im konzentrischen und exzentrischen horizontalen Ringspalt zwischen zwei Zylindern, der mit zwei nichtmischbaren Fluiden (Wasser/Luft, Wasser/Silikonöl 10, Wasser/Silikonöl 100, Frigen 113/Wasser) gefüllt ist, untersucht. Die Verteilungen von Stromfunktion und Temperatur, die örtlichen und mittleren äquivalenten Wärmeleitfähigkeiten, werden in einem weiten Bereich der Rayleighzahl angegeben. Der Einfluß thermokapillarer Konvektion (Marangonikonvektion) wird am System Wasser/Luft, unter sonst gleicher geometrischer Konfiguration, aufgezeigt.

ТЕПЛООБМЕН ПРИ ТЕРМОГРАВИТАЦИОННОЙ И ТЕРМОКАПИЛЛЯРНОЙ КОНВЕКЦИИ В КОНЦЕНТРИЧЕСКОМ И ЭКСЦЕНТРИЧЕСКОМ КОЛЬЦЕВЫХ КАНАЛАХ, ЗАПОЛНЕННЫХ ДВУМЯ НЕСМЕШИВАЮЩИМИСЯ ЖИДКОСТЯМИ

Аннотация—Приводятся численные расчеты ламинарной термогравитационной конвекции в концентрических и эксцентрических горизонтальных цилиндрических кольцевых каналах, заполненных двумя несмешивающимися жидкостями (вода–воздух, вода–силиконовое масло 10, вода–силиконовое масло 100, Фреон 113–вода). Поля скоростей и температуры, локальные и средние эквивалентные значения теплопроводности найдены для широкого диапазона чисел Рэлея. Кроме того, рассматривается влияние термокапиллярной конвекции (конвекция Марангони) в кольцевом канале для системы вода–воздух.